

Two-dimensional non-Hermitian fermionic superfluidity with spin imbalanceTingting Shi,^{1,2,3} Siqi Wang,² Zhiyue Zheng,^{1,*} and Wei Zhang^{2,3,1,†}¹*Beijing Academy of Quantum Information Sciences, Beijing 100193, China*²*Department of Physics and Beijing Key Laboratory of Opto-electronic Functional Materials and Micro-nano Devices, Renmin University of China, Beijing 100872, China*³*Key Laboratory of Quantum State Construction and Manipulation (Ministry of Education), Renmin University of China, Beijing 100872, China*

(Received 7 March 2024; accepted 17 May 2024; published 3 June 2024)

The two-body loss associated with inelastic interactions between fermions plays a significant role in realistic many-body systems. Here we study a two-component non-Hermitian Bardeen-Cooper-Schrieffer superfluidity with spin imbalance and two-body loss characterized by a complex-valued s -wave interaction in a square lattice. At the mean-field level, we map out the zero-temperature phase diagram and observe a dissipation-induced transition from superfluid to normal phase as well as a distinctive revival of the superfluid state in the weakly interacting regime applicable to both spin-balanced and spin-imbalanced systems. In the spin-imbalanced case, we find that the effective density of states involving weight functions reduces the regions in \mathbf{k} space contributing to pairing, hence leading to a pronounced expansion of the normal phase on the phase diagram. Additionally, we analyze the order parameter, condensate energy, quasiparticle spectra, momentum distribution, and compressibility to characterize the presenting phases and phase transitions.

DOI: [10.1103/PhysRevA.109.063306](https://doi.org/10.1103/PhysRevA.109.063306)**I. INTRODUCTION**

In the realm of quantum mechanics, Hermiticity stands as a fundamental postulate in the description of closed quantum systems. It ensures real-valued energy expectations and unitary time evolutions. However, a physical system under realistic conditions is usually coupled with the environment, so the formalism of a Hermitian Hamiltonian becomes compromised. To address this challenge, theories employing the Lindblad equation instead of the Schrödinger equation have been developed to describe the evolution of open quantum systems [1,2]. Alternatively, a non-Hermitian Hamiltonian is considered as a simple yet powerful approximation, which can successfully capture many essential features of open quantum systems provided the contribution from terms involving jump operators are negligible. Over the past several decades, the study of non-Hermitian Hamiltonians has aroused a great deal of interest from both experimental and theoretical communities [1–18] and has revealed rich exotic phenomena such as exceptional points [12,13], the quantum Zeno effect [7,15], and quantum critical phenomena [16,17]. One notable area of interest is the investigation of non-Hermitian Hamiltonians with parity-time-reversal symmetry [19], which have been realized and intensively studied in a variety of physical systems, including microcavities [8], waveguides [9], optical systems [17], cold atoms [18], and trapped ions [13,14]. While much knowledge of single-particle behavior has been gained from

these pioneering works, less attention has been paid to non-Hermitian many-body systems.

Two of the most fascinating and profound phenomena of many-body physics are fermionic superconductivity and superfluidity [20–32]. Despite being discovered more than a century ago, they remain on the very frontier of research in multidisciplinary fields of physics, including condensed-matter physics, nuclear physics, astrophysics, and ultracold-atom physics [33]. In diverse systems, fermions of different spins or pseudospins can pair with each other under effectively attractive interactions, and the pairs will behave collectively at low enough temperature to form a macroscopic quantum state and sustain coherent transport. Most existing theories of such a mechanism consider only elastic interactions between fermions, with the many-body Hamiltonian being inherently Hermitian. However, in many experimental setups, the interactions can possess inelastic channels as fermions are scattered out of the considered Hilbert space. For example, in ultracold quantum gases, two fermionic atoms at designated hyperfine levels, considered as pseudospins, can undergo inelastic scattering to two other hyperfine levels and become dark to lasers or get lost from the trap. In both cases, the inelastic processes result in a loss of particles, rendering the system open. To study fermionic superfluid under inelastic interactions, a non-Hermitian many-body Hamiltonian with a complex-valued interaction is adopted and analyzed within a mean-field approach for both a three-dimensional lattice model [29] and a continuum system [31]. Later, the discussion is also extended to one-dimensional gases with p -wave interaction to account for the relatively high loss rate [32]. Restricted within balanced-spin populations and at zero temperature, a revival of superfluidity is observed for all cases.

*zhengzy@baqis.ac.cn

†wzhangl@ruc.edu.cn

Here we consider a two-dimensional (2D) fermionic system on a square lattice with an s -wave complex-valued interaction. By allowing an imbalance of spin populations, we calculate the ground state of the system at zero temperature within a mean-field approach and map out the phase diagram showing the competition between superfluid and normal phases. In the weak-interaction regime, we uncover a dissipation-induced superfluid to normal phase transition and a remarkable revival of superfluid state. In addition, the inclusion of spin imbalance modifies the density of states (DOS) and reduces the pairing effect, leading to an expanded normal phase. The physical properties of such phases and phase transitions can be characterized by measurements of quasiparticle spectra, momentum distribution of particles, and compressibility, which are calculated and discussed.

The remainder of this paper is organized as follows. In Sec. II we introduce the effective non-Hermitian Hamiltonian and derive the thermodynamical potential under mean-field approximation. In Sec. III we focus on the zero-temperature limit and map out the phase diagram by analyzing the condensate energy and superfluid order parameter. In Sec. IV we present the quasiparticle spectra, momentum distribution, and compressibility to characterize the phases and phase transitions. We summarize in Sec. V.

II. MODEL HAMILTONIAN AND MEAN-FIELD APPROACH

We consider a two-component Fermi system in a 2D square lattice with lattice constant d , where particles with opposite pseudospins attractively interact via an s -wave contact interaction [29]. The Hamiltonian is written as

$$\hat{H} = \sum_{\mathbf{k}\sigma} \xi_{\mathbf{k},\sigma} c_{\mathbf{k},\sigma}^\dagger c_{\mathbf{k},\sigma} - \frac{U}{N} \sum_{\mathbf{k}\mathbf{k}'\mathbf{q}} c_{\mathbf{k}+\mathbf{q}/2,\uparrow}^\dagger c_{-\mathbf{k}+\mathbf{q}/2,\downarrow}^\dagger c_{-\mathbf{k}'+\mathbf{q}/2,\downarrow} c_{\mathbf{k}'+\mathbf{q}/2,\uparrow}. \quad (1)$$

Here $c_{\mathbf{k},\sigma}$ and $c_{\mathbf{k},\sigma}^\dagger$ are the annihilation and creation fermionic operators, respectively, with the 2D dispersion relation $\varepsilon_{\mathbf{k}} = -2t[\cos(k_x d) + \cos(k_y d)]$ and hopping strength t , $\xi_{\mathbf{k},\sigma} = \varepsilon_{\mathbf{k}} - \mu_\sigma$ is the shifted dispersion by the spin-dependent chemical potential μ_σ , and N denotes the number of lattice sites. The interaction $U = U_1 + i\frac{\gamma}{2}$ is assumed to be complex, incorporating the interaction strength U_1 and the two-body loss rate γ . Adopting the extended Bardeen-Cooper-Schrieffer (BCS) theory for non-Hermitian systems, we consider a mean-field pairing order parameter with center-of-mass momentum \mathbf{q} , defined as

$$\Delta = -\frac{U}{N} \sum_{\mathbf{k}} L \langle c_{-\mathbf{k}+\mathbf{q}/2,\downarrow} c_{\mathbf{k}+\mathbf{q}/2,\uparrow} \rangle_R = \Delta_0 e^{i\mathbf{q}\cdot\mathbf{r}},$$

$$\tilde{\Delta} = -\frac{U}{N} \sum_{\mathbf{k}} L \langle c_{\mathbf{k}+\mathbf{q}/2,\uparrow}^\dagger c_{-\mathbf{k}+\mathbf{q}/2,\downarrow}^\dagger \rangle_R = \Delta_0 e^{-i\mathbf{q}\cdot\mathbf{r}}. \quad (2)$$

Note that Δ and $\tilde{\Delta}$ are not complex conjugate to each other given that Δ_0 is generally a complex number. The mean-field

Hamiltonian is expressed as

$$\hat{H}_{\text{MF}} = \frac{N}{U} \Delta \tilde{\Delta} + \sum_{\mathbf{k}} (\xi_{\mathbf{k}+\mathbf{q}/2,\uparrow} c_{\mathbf{k}+\mathbf{q}/2,\uparrow}^\dagger c_{\mathbf{k}+\mathbf{q}/2,\uparrow} + \xi_{-\mathbf{k}+\mathbf{q}/2,\downarrow} c_{-\mathbf{k}+\mathbf{q}/2,\downarrow}^\dagger c_{-\mathbf{k}+\mathbf{q}/2,\downarrow}) + \sum_{\mathbf{k}} (\Delta c_{\mathbf{k}+\mathbf{q}/2,\uparrow}^\dagger c_{-\mathbf{k}+\mathbf{q}/2,\downarrow}^\dagger + \tilde{\Delta} c_{-\mathbf{k}+\mathbf{q}/2,\downarrow} c_{\mathbf{k}+\mathbf{q}/2,\uparrow}), \quad (3)$$

which can be diagonalized as

$$\hat{H}_{\text{MF}} = \sum_{\mathbf{k}} (E_{\mathbf{k}\mathbf{q},+} \alpha_{\mathbf{k}+\mathbf{q}/2,\uparrow}^\dagger \alpha_{\mathbf{k}+\mathbf{q}/2,\uparrow} - E_{\mathbf{k}\mathbf{q},-} \bar{\alpha}_{-\mathbf{k}+\mathbf{q}/2,\downarrow}^\dagger \bar{\alpha}_{-\mathbf{k}+\mathbf{q}/2,\downarrow}) + \sum_{\mathbf{k}} (\xi_{-\mathbf{k}+\mathbf{q}/2,\downarrow} + E_{\mathbf{k}\mathbf{q},-}) + \frac{N}{U} \Delta \tilde{\Delta} \quad (4)$$

with the aid of the Bogoliubov transformation

$$\begin{pmatrix} \alpha_{\mathbf{k}+\mathbf{q}/2,\uparrow} \\ \bar{\alpha}_{-\mathbf{k}+\mathbf{q}/2,\downarrow} \end{pmatrix} = \begin{pmatrix} u_{\mathbf{k}\mathbf{q}} & -v_{\mathbf{k}\mathbf{q}} \\ \bar{v}_{\mathbf{k}\mathbf{q}} & u_{\mathbf{k}\mathbf{q}} \end{pmatrix} \begin{pmatrix} c_{\mathbf{k}+\mathbf{q}/2,\uparrow} \\ c_{-\mathbf{k}+\mathbf{q}/2,\downarrow}^\dagger \end{pmatrix}, \quad (5)$$

where α and $\bar{\alpha}$ are quasiparticle operators. The coefficients within the transformation are

$$u_{\mathbf{k}\mathbf{q}} = \sqrt{\frac{E_{\mathbf{k}\mathbf{q}} + \xi_{\mathbf{q},+}}{2E_{\mathbf{k}\mathbf{q}}}},$$

$$v_{\mathbf{k}\mathbf{q}} = \sqrt{\frac{E_{\mathbf{k}\mathbf{q}} - \xi_{\mathbf{q},+}}{2E_{\mathbf{k}\mathbf{q}}}} \sqrt{\frac{\Delta}{\tilde{\Delta}}},$$

$$\bar{v}_{\mathbf{k}\mathbf{q}} = \sqrt{\frac{E_{\mathbf{k}\mathbf{q}} - \xi_{\mathbf{q},+}}{2E_{\mathbf{k}\mathbf{q}}}} \sqrt{\frac{\tilde{\Delta}}{\Delta}}, \quad (6)$$

where $E_{\mathbf{k}\mathbf{q}} = \sqrt{\xi_{\mathbf{q},+}^2 + \Delta \tilde{\Delta}}$ and $\xi_{\mathbf{q},+} = (\xi_{\mathbf{k}+\mathbf{q}/2,\uparrow} + \xi_{-\mathbf{k}+\mathbf{q}/2,\downarrow})/2$. The eigenenergies of the quasiparticles are $E_{\mathbf{k}\mathbf{q},\pm} = (\xi_{\mathbf{k}+\mathbf{q}/2,\uparrow} - \xi_{-\mathbf{k}+\mathbf{q}/2,\downarrow})/2 \pm E_{\mathbf{k}\mathbf{q}}$. Considering the static properties of quasiparticles $\alpha^\dagger \alpha = 0$ or 1, we reach the grand partition function

$$\mathcal{Z}_{\text{MF}} = \prod_{\mathbf{k}} [(1 + e^{-\beta E_{\mathbf{k}\mathbf{q},+}})(1 + e^{\beta E_{\mathbf{k}\mathbf{q},-}}) \times e^{-\beta(\xi_{-\mathbf{k}+\mathbf{q}/2,\downarrow} + E_{\mathbf{k}\mathbf{q},-})}] e^{-\beta(N/U)\Delta\tilde{\Delta}}, \quad (7)$$

where $\beta = 1/k_B T$ denotes the inverse temperature. The thermodynamic potential obtained from $\Omega_{\text{MF}} = -\frac{1}{\beta} \ln \mathcal{Z}_{\text{MF}}$ then reads

$$\Omega_{\text{MF}} = -\frac{1}{\beta} \sum_{\mathbf{k}} \ln(1 + e^{-\beta E_{\mathbf{k}\mathbf{q},+}})(1 + e^{\beta E_{\mathbf{k}\mathbf{q},-}}) + \sum_{\mathbf{k}} (\xi_{-\mathbf{k}+\mathbf{q}/2,\downarrow} + E_{\mathbf{k}\mathbf{q},-}) + \frac{N}{U} \Delta \tilde{\Delta}. \quad (8)$$

In the following discussion, we focus on the most representative case of zero center-of-mass momentum, corresponding to the conventional BCS superfluid phase. The general case of a finite center-of-mass momentum, known as the Fulde-Ferrell-Larkin-Ovchinnikov (FFLO) phase, is suggested to exist only within a limited parameter space of interaction

strength and particle filling such that the energy cost of the spatially varying order parameter can be compensated by the gain of condensation energy [34,35]. The presence of dissipation tends to reduce the condensation energy and hence is unfavorable to the existence of the FFLO state. By assigning $\mathbf{q} = \mathbf{0}$ we get

$$\Omega_{\text{MF}} = -\frac{1}{\beta} \sum_{\mathbf{k}} \ln(1 + e^{-\beta E_{\mathbf{k},+}})(1 + e^{\beta E_{\mathbf{k},-}}) + \sum_{\mathbf{k}} (\xi_{-\mathbf{k},\downarrow} + E_{\mathbf{k},-}) + \frac{N}{U} \Delta_0^2, \quad (9)$$

where $E_{\mathbf{k},\pm} = \frac{\xi_{\mathbf{k},\uparrow} - \xi_{-\mathbf{k},\downarrow}}{2} \pm \sqrt{(\frac{\xi_{\mathbf{k},\uparrow} + \xi_{-\mathbf{k},\downarrow}}{2})^2 + \Delta_0^2} = -\frac{\delta\mu}{2} \pm \sqrt{(\varepsilon_{\mathbf{k}} - \bar{\mu})^2 + \Delta_0^2}$. Here $\delta\mu = \mu_{\uparrow} - \mu_{\downarrow}$ and $\bar{\mu} = (\mu_{\uparrow} + \mu_{\downarrow})/2$ are the difference and average of chemical potentials of the two spin states, respectively. Owing to the time-reversal symmetry between the two spin states, we consider only the case of a non-negative $\delta\mu$.

III. ZERO-TEMPERATURE PHASE DIAGRAM

At zero temperature, we can further simplify the thermodynamic potential by reducing the Fermi function to the Heaviside step function

$$\Omega_{\text{MF}} = \sum_{\mathbf{k}} [E_{\mathbf{k},+} \Theta(-E_{\mathbf{k},+}) - E_{\mathbf{k},-} \Theta(E_{\mathbf{k},-}) + \xi_{-\mathbf{k},\downarrow} + E_{\mathbf{k},-}] + \frac{N}{U} \Delta_0^2. \quad (10)$$

In our numerical calculations, we adopt the hopping integral t and lattice constant d as units of energy and length, respectively.

To derive the zero-temperature phase diagram, we obtain the gap equation from the stationary condition $\partial S_{\text{eff}}/\partial \Delta|_{\Delta=\Delta_0} = 0$, yielding

$$\frac{N}{U} = \sum_{\mathbf{k}} \frac{1}{2E_{\mathbf{k}}} [\Theta(-E_{\mathbf{k},-}) - \Theta(-E_{\mathbf{k},+})]. \quad (11)$$

For definiteness, we consider the case of half filling with the average chemical potential $\bar{\mu} = 0$, so that the total number of particles is equal to the number of lattice sites. The order parameters are obtained by solving the gap equation (11) for different choices of interaction strength U_1 and dissipation γ . To distinguish different phases, we resort to the condensate energy, defined as the energy difference between the superfluid state and the normal state as $\Delta E \equiv \Omega_{\text{MF}}(\Delta_0) - \Omega_{\text{MF}}(0)$. A solution with finite order parameters and $\text{Re}(\Delta E) < 0$ signifies the ground state of the system as a superfluid state (SF). Conversely, $\text{Re}(\Delta E) > 0$ suggests a stable normal state as the ground state, while the finite superfluid order parameter is identified as a metastable superfluid phase (MSF). If Eq. (11) does not have any finite-value solution for the order parameter, the system is in the normal phase [denoted by N in Fig. 1(a)].

Based on these criteria, we map out the zero-temperature phase diagrams on the U_1 - γ plane and elucidate the intricate interplay between the interaction strength, dissipation, and chemical potential difference, as depicted in Fig. 1. Specifically, Fig. 1(a) illustrates the scenario for $\delta\mu/t = 0$, where

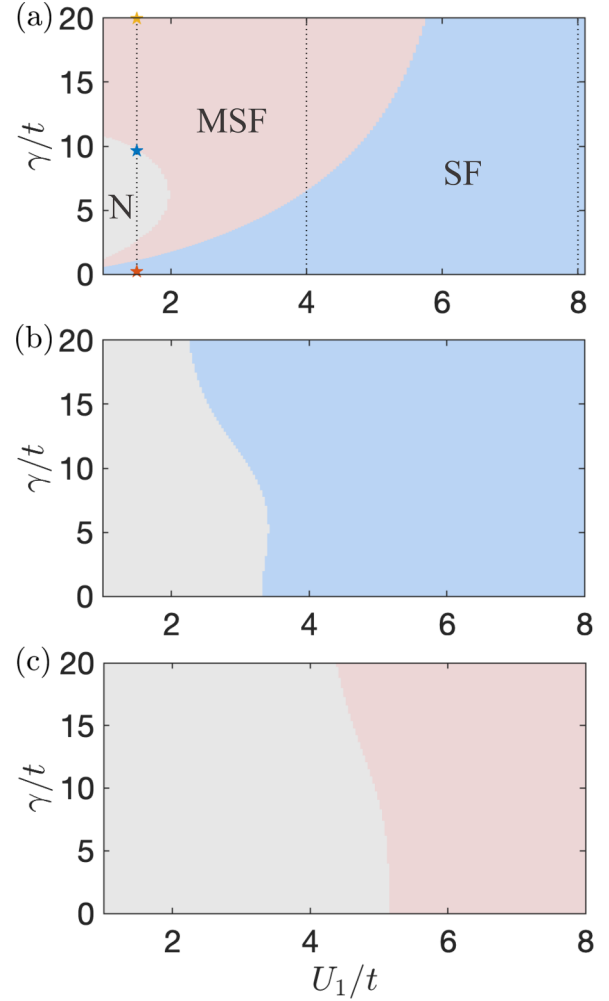


FIG. 1. Zero-temperature phase diagram by varying the interaction strength U_1 and the dissipation γ with the chemical potential difference: (a) $\delta\mu/t = 0$, (b) $\delta\mu/t = 2$, and (c) $\delta\mu/t = 4$. The blue, red, and gray regions denote stable superfluid, metastable superfluid, and normal states, respectively.

three phases can be identified. In the regime of sufficiently strong attractive interaction, fermions form tightly bound bi-atomic molecules, which couple with each other coherently to support a superfluid state denoted by the blue region. At intermediate interaction strengths, the system transits from the SF to the MSF state, marked in red, as dissipation increases. The most striking feature is the revival of the superfluid state in the weakly interacting regime. When the dissipation is small, fermions with different spins pair with each other to host superfluidity. With increasing dissipation, the system suffers severe particle loss via inelastic collision when one particle hops to a neighboring site occupied by another particle. This process drives the system into the normal phase, denoted by gray in the phase diagram. However, when the dissipation is further increased, particle hopping between neighboring sites is suppressed such that an on-site tightly bound molecule is formed to inhibit two-body loss from inelastic collisions, thus prompting the system to reenter the MSF phase. The stark phenomenon that strong dissipation inhibits two-body loss has been observed in several experimental works [36,37] and

can be interpreted as a manifestation of the quantum Zeno effect (QZE) [7,38]. The conventional QZE is defined as the suppression of decay rate by frequent applications of measurement. The concept of the QZE has also been generalized to the case of continuous measurement, and an equivalence condition between continuous and discrete measurements has been established [39]. In the present problem, the strong on-site dissipation serves as a continuous measurement to suppress the coherent particle tunneling and inhibit particle loss. The revival of superfluidity attributed to the QZE in a lattice has also been observed in continuum models [31,32].

Another characteristic feature of this phase diagram is that the transition between the (metastable) superfluid state and the normal state does not belong to the universality class of a conventional $U(1)$ gauge symmetry-breaking phase transition. On the contrary, it is associated with the spontaneous breaking of parity–particle-hole (CP) symmetry at the exceptional points where the order parameters are purely imaginary and the effective Hamiltonian cannot be diagonalized. In general, this phase transition cannot even be classified as a first- or second-order phase transition based on Ehrenfest’s classification since it is rooted in the appearance of exceptional points and is typical in a non-Hermitian system.

In the case of spin-imbalanced populations, the Heaviside functions in Eq. (11) act as weight functions for the order parameter and lead to an effective DOS which restricts the regions in \mathbf{k} space for pairing. As a consequence, the region of the normal state expands and the disappearance and restoration of superfluidity occurs in a narrower parameter window of U_1 upon elevating the chemical potential difference $\delta\mu$. These can be seen in Fig. 1 for different chemical differences $\delta\mu$. In particular, by comparing Figs. 1(b) and 1(c) we find that the superfluid will become unstable with increasing chemical potential difference, even when the attraction is extremely strong.

To gain deep insights into the phase diagram, we present the order parameter Δ_0/t and the condensate energy as functions of dissipation γ with $\delta\mu = 0$ in Fig. 2, choosing three typical interaction strengths U_1 indicated by vertical black dotted lines in Fig. 1(a). As shown in Fig. 2(ai), in the regime of weak interaction, the superfluid state is destroyed with increasing dissipation, leading to the system being in the normal state. Nevertheless, as dissipation is further enhanced, the superfluid state begins to recover and the order parameter increases and converges to $\Delta_0 = U/2$ in the strong dissipation limit. In this limit, the coherent process of hopping between nearest-neighbor sites is greatly suppressed due to the QZE, resulting in the localization of fermion pairs and the formation of molecules. This suggests that the physical property of the system is dominantly determined by the on-site interaction, which is consistent with the asymptotic value of the order parameter. In Fig. 2(aii) we observe that the condensate energy is negative in the weak-dissipation regime but becomes positive and approaches $\Delta E = 16t/\pi^2 - U/4$ in the strong-dissipation regime, indicative of a stable and a metastable superfluid state in these two regimes, respectively.

When the interaction strength is intermediate, a stronger pairing effect can overcome the detrimental mechanisms of particle loss via inelastic collision and pair dissociation by inter-site hopping such that the normal state disappears and

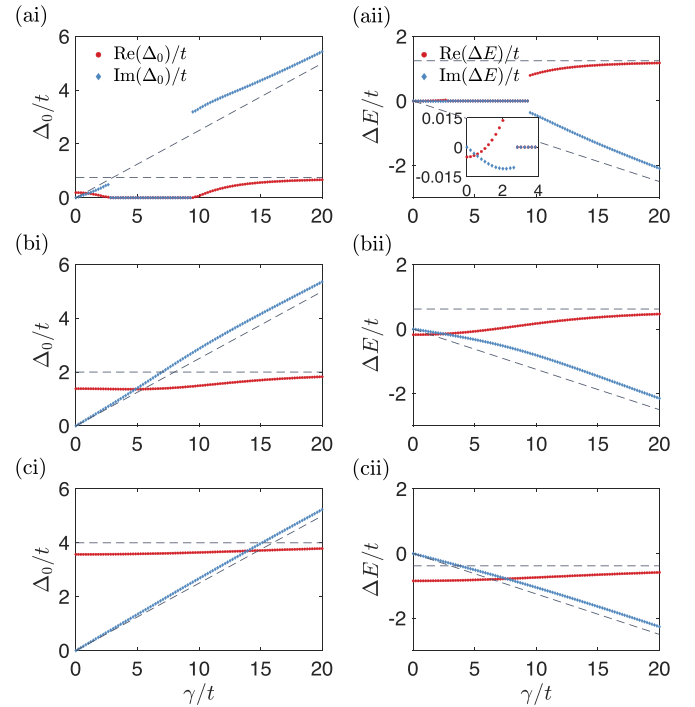


FIG. 2. Plots of the real parts (red circles) and imaginary parts (blue diamonds) of (i) order parameter Δ_0/t and (ii) condensate energy $\Delta E/t$ (right column) as functions of dissipation γ/t at zero temperature. The adopted interaction strengths are (a) $U_1/t = 1.5$, (b) $U_1/t = 4$, and (c) $U_1/t = 8$, corresponding to the vertical black dotted lines in Fig. 1(a), respectively. The black dashed lines represent the asymptotic behaviors in the strong dissipation limit, i.e., $\Delta_0(\gamma/t \rightarrow +\infty) = U/2$ and $\Delta E(\gamma/t \rightarrow +\infty) = 16t/\pi^2 - U/4$. The inset shows a close-up of weak interaction in the range of weak dissipation.

the superfluid state persists across the range of dissipation, as shown in Fig. 2(b). In the strong-interaction region with $U_1/t = 8$ illustrated in Fig. 2(c), the interaction strength exceeds the critical value $U_1^c = 64t/\pi^2$ and the real part of the condensate energy converges to $\text{Re}(\Delta E) \rightarrow (16/\pi^2 - 2)t < 0$ from below in the large- γ limit. In addition, the tightly bound molecules in the strong-attraction regime can avoid decoherence caused by dissipation. Therefore, the superfluid remains stable for arbitrary dissipation.

IV. QUASIPARTICLE SPECTRA, MOMENTUM DISTRIBUTION, AND COMPRESSIBILITY

To gain a better understanding of the revival of superfluidity in the weak-interaction regime, we calculate the quasiparticle energy spectra $E_{\mathbf{k},\pm}$ in different phases with $\delta\mu = 0$ and present the results in Fig. 3. From top to bottom, the plots show the cases labeled by stars in Fig. 1(a). The real and imaginary parts of quasiparticle spectra characterize the quasiparticle excitation energy and lifetime, respectively. Figures 3(ai) and 3(ci) reveal that the energy bands are always gapped in both SF and MSF phases. However, the two bands touch to form exceptional lines at the transition point, as demonstrated in Fig. 3(b). The spectra with unbroken CP symmetry are purely imaginary between the exceptional

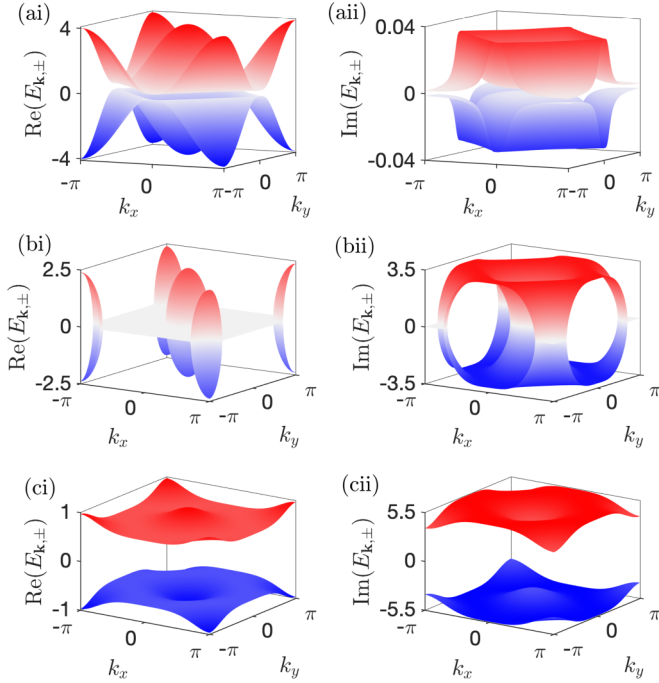


FIG. 3. (i) Real parts and (ii) imaginary parts of quasiparticle energy spectra $E_{\mathbf{k},\pm}$ with $\delta\mu = 0$. The order parameters are (a) $\Delta_0/t = 0.188 + 0.033i$ (stable superfluid state), (b) $\Delta_0/t = 3.193i$ (phase transition point), and (c) $\Delta_0/t = 0.668 + 5.434i$ (metastable superfluid state), as marked by stars in Fig. 1(a).

lines, while they become anticonjugate complex inside the exceptional lines, where CP symmetry is spontaneously broken. This indicates that quasiparticles can be stimulated by a nonzero excitation energy and will be dissipated in SF [Fig. 3(a)] and MSF [Fig. 3(c)] phases. However, at the transition point [Fig. 3(b)], an infinitesimally small energy suffices to excite quasiparticles, allowing them to remain in an excited state. Moreover, as depicted in Figs. 3(c), strong dissipations significantly reduce the band width and enlarge the energy gap, which is consistent with our expectation of the localization of on-site molecules due to the QZE and the enhancement of the order parameter.

We also explore the zero-temperature momentum distribution for $\delta\mu = 0$, given by $n_{\mathbf{k},\uparrow} = n_{\mathbf{k},\downarrow} = (1 - \xi_{\mathbf{k}}/E_{\mathbf{k}})/2$. The momentum distributions for three characteristic sets of parameters, corresponding to those in Fig. 3, are presented in Fig. 4. In the SF phase with weak dissipation, as shown in Fig. 4(a), the momentum distribution exhibits a Fermi-Dirac-like behavior, albeit slightly deformed in the vicinity of the Fermi surface due to an interplay between the weak attraction and weak dissipation. In contrast, the MSF phase with strong dissipation, illustrated in Fig. 4(c), displays a nearly uniform momentum distribution. This observation provides additional evidence of the localization of particles and the formation of bosonic molecules at individual sites. At the critical point, particles tend to congregate on the exceptional lines due to its low energy and long lifetime. This leads to the divergence of momentum distribution, as depicted in Fig. 4(b).

The pronounced rearrangement of divergent behavior of the momentum distribution on the exceptional lines leaves a

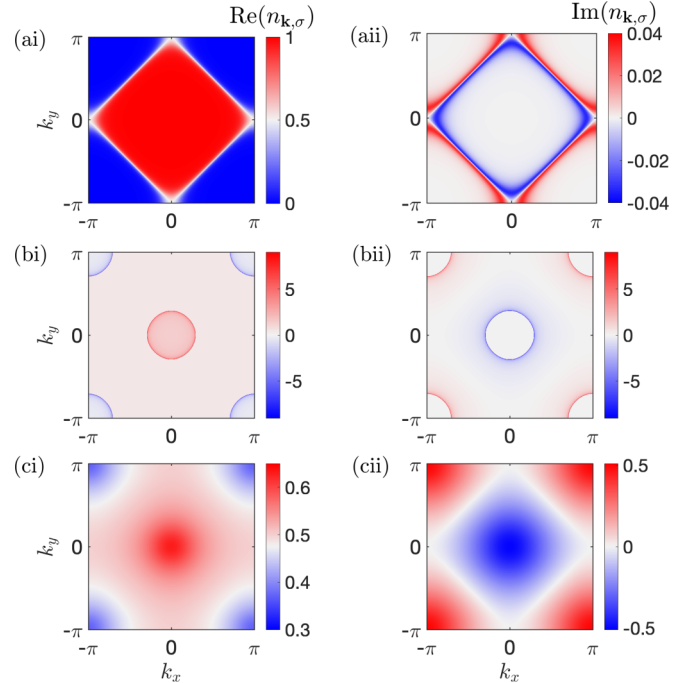


FIG. 4. Momentum distribution of quasiparticles. All parameters are the same as in the corresponding panels in Fig. 3.

distinctive imprint on the isothermal electronic compressibility, which is directly linked to quasiparticle energy spectra and momentum distribution. The compressibility is defined as $\kappa = -(L^2/N_0^2)\partial^2\Omega/\partial\mu^2$, where N_0 is the total particle number and L represents the characteristic length of the system. Under the conditions of zero temperature and half filling, the compressibility can be further expressed as

$$\kappa = \frac{L^2}{N^2} \sum_{\mathbf{k}} \frac{\Delta_0^2}{E_{\mathbf{k}}^3} \Theta(E_{\mathbf{k},+}). \quad (12)$$

In Fig. 5 we present the compressibility as a function of dissipation with the interaction strength fixed at $U_1/t = 1.5$ for various chemical potential differences. As dissipation γ increases, there exist discontinuities at phase transition points in compressibility, which can be used to detect the phase transition from the superfluid state to the normal state. We emphasize that although the discontinuity in compressibility is similar to what one would observe in a conventional superfluid-normal phase transition, here the true nature of the transition originates from the exceptional points and hence cannot be simply classified as a second-order phase transition. When we continue to increase γ to the strong dissipation regime, the compressibility decreases continuously. This tendency can be understood by noticing that a strong enough dissipation can localize particles due to the QZE such that the superfluid becomes incompressible. Notably, as the chemical potential difference is increased, the parameter range associated with the normal state is further expanded since the effective DOS will suppress pairing. This qualitative observation is in good agreement with our analysis before. In experiments on atomic quantum gases, the measurement of isothermal compressibility can be conducted by measuring particle density fluctuations in a grand canonical ensemble via

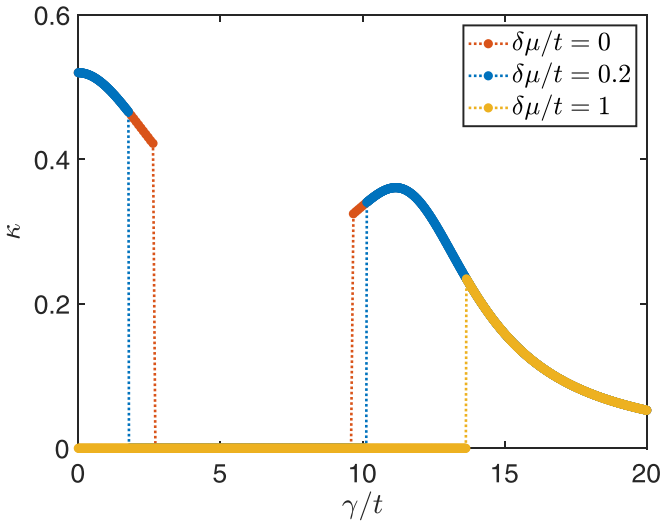


FIG. 5. Plot of compressibility against dissipation. The curves are obtained when the interaction strength is fixed at $U_1/t = 1.5$ and the chemical potential differences are $\delta\mu/t = 0$ (red dotted line), $\delta\mu/t = 0.2$ (blue dotted line), and $\delta\mu = 1$ (yellow dotted line). The discontinuities in compressibility signify the superfluid to normal phase transition.

the thermodynamical formula $\kappa = L^2(\langle N_0^2 \rangle - \langle N_0 \rangle^2)/T \langle N_0 \rangle^2$ [40,41], where $\langle N_0 \rangle$ is the average number of particles.

V. CONCLUSION

We have investigated the zero-temperature phase diagram and fundamental properties of a two-component fermionic

system in two-dimensional square lattices, considering spin-imbalanced populations and inelastic two-body loss characterized by an s -wave complex-valued interaction. Within a mean-field approximation, we mapped out the phase diagram by solving the gap equation and calculating the condensate energy. Notably, in the weak-interaction regime, we uncovered a dissipation-induced superfluid to normal phase transition and a remarkable revival of the superfluid state attributed to the quantum Zeno effect. In addition, the introduction of spin-imbalanced populations can modify the density of states and hence suppresses the pairing effect and favors the normal phase in a larger parameter regime on the phase diagram. Finally, we calculated quasiparticle spectra, the momentum distribution of particles, and compressibility as characteristic physical properties of such phases and phase transitions. As an outlook, we point out that our analysis of s -wave superfluid can be extended to investigate the stability of the p - or d -wave superfluid state, in which cases the two-body loss of inelastic collision is more prominent. It would also be interesting to study the possibility of other exotic pairing phases, such as the finite center-of-mass momentum pairing state and the breached paired phase. To get a closer connection to realistic experimental conditions, it is desirable to incorporate the effect of quantum jump terms via the Lindblad equation.

ACKNOWLEDGMENTS

This work was supported by the National Natural Science Foundation of China (Grants No. 12074428 and No. 92265208) and the National Key R&D Program of China (Grant No. 2022YFA1405301). T.S. is grateful for support from the Postdoctoral Fellowship Program of CPSF (Grant No. GZC20232945).

-
- [1] Y. Ashida, Z. Gong, and M. Ueda, *Adv. Phys.* **69**, 249 (2020).
 - [2] A. J. Daley, *Adv. Phys.* **63**, 77 (2014).
 - [3] N. Hatano and D. R. Nelson, *Phys. Rev. Lett.* **77**, 570 (1996).
 - [4] C. M. Bender and S. Boettcher, *Phys. Rev. Lett.* **80**, 5243 (1998).
 - [5] C. M. Bender, D. C. Brody, and H. F. Jones, *Phys. Rev. Lett.* **89**, 270401 (2002).
 - [6] C. M. Bender, *Rep. Prog. Phys.* **70**, 947 (2007).
 - [7] B. Zhu, B. Gadway, M. Foss-Feig, J. Schachenmayer, M. L. Wall, K. R. A. Hazzard, B. Yan, S. A. Moses, J. P. Covey, D. S. Jin, J. Ye, M. Holland, and A. M. Rey, *Phys. Rev. Lett.* **112**, 070404 (2014).
 - [8] W. Chen, Ş. K. Özdemir, G. Zhao, J. Wiersig, and L. Yang, *Nature (London)* **548**, 192 (2017).
 - [9] R. El-Ganainy, K. G. Makris, M. Khajavikhan, Z. H. Musslimani, S. Rotter, and D. N. Christodoulides, *Nat. Phys.* **14**, 11 (2018).
 - [10] V. M. Martinez Alvarez, J. E. Barrios Vargas, and L. E. F. Foa Torres, *Phys. Rev. B* **97**, 121401(R) (2018).
 - [11] N. Okuma, K. Kawabata, K. Shiozaki, and M. Sato, *Phys. Rev. Lett.* **124**, 086801 (2020).
 - [12] W. D. Heiss, *J. Phys. A: Math. Theor.* **45**, 444016 (2012).
 - [13] L. Ding, K. Shi, Q. Zhang, D. Shen, X. Zhang, and W. Zhang, *Phys. Rev. Lett.* **126**, 083604 (2021).
 - [14] L. Ding, K. Shi, Y. Wang, Q. Zhang, C. Zhu, L. Zhang, J. Yi, S. Zhang, X. Zhang, and W. Zhang, *Phys. Rev. A* **105**, L010204 (2022).
 - [15] J. Li, T. Wang, L. Luo, S. Vemuri, and Y. N. Joglekar, *Phys. Rev. Res.* **5**, 023204 (2023).
 - [16] K. Kawabata, Y. Ashida, and M. Ueda, *Phys. Rev. Lett.* **119**, 190401 (2017).
 - [17] L. Xiao, K. Wang, X. Zhan, Z. Bian, K. Kawabata, M. Ueda, W. Yi, and P. Xue, *Phys. Rev. Lett.* **123**, 230401 (2019).
 - [18] J. Li, A. K. Harter, J. Liu, L. de Melo, Y. N. Joglekar, and L. Luo, *Nat. Commun.* **10**, 855 (2019).
 - [19] C. M. Bender and D. W. Hook, [arXiv:2312.17386](https://arxiv.org/abs/2312.17386)
 - [20] J. Bardeen, L. N. Cooper, and J. R. Schrieffer, *Phys. Rev.* **106**, 162 (1957).
 - [21] J. Bardeen, L. N. Cooper, and J. R. Schrieffer, *Phys. Rev.* **108**, 1175 (1957).
 - [22] A. J. Leggett, *J. Phys. (Paris) Colloq.* **41**, C7-19 (1980).
 - [23] A. J. Leggett, in *Low Temperature Physics*, edited by M. J. R. Hoch and R. H. Lemmer, Lecture Notes in Physics Vol. 394 (Springer, Berlin, 1991), pp. 1–92.

- [24] P. Nozières and S. Schmitt-Rink, *J. Low Temp. Phys.* **59**, 195 (1985).
- [25] C. A. R. Sá de Melo, M. Randeria, and J. R. Engelbrecht, *Phys. Rev. Lett.* **71**, 3202 (1993).
- [26] N. M. Chtchelkatchev, A. A. Golubov, T. I. Baturina, and V. M. Vinokur, *Phys. Rev. Lett.* **109**, 150405 (2012).
- [27] A. Ghatak and T. Das, *Phys. Rev. B* **97**, 014512 (2018).
- [28] L. Zhou and X. Cui, *iScience* **14**, 257 (2019).
- [29] K. Yamamoto, M. Nakagawa, K. Adachi, K. Takasan, M. Ueda, and N. Kawakami, *Phys. Rev. Lett.* **123**, 123601 (2019).
- [30] K. Yamamoto, M. Nakagawa, N. Tsuji, M. Ueda, and N. Kawakami, *Phys. Rev. Lett.* **127**, 055301 (2021).
- [31] M. Iskin, *Phys. Rev. A* **103**, 013724 (2021).
- [32] H. Tajima, Y. Sekino, D. Inotani, A. Dohi, S. Nagataki, and T. Hayata, *Phys. Rev. A* **107**, 033331 (2023).
- [33] C. A. R. Sá de Melo, *Phys. Today* **61** (10), 45 (2008).
- [34] W. Zhang and L.-M. Duan, *Phys. Rev. A* **76**, 042710 (2007).
- [35] L. Radzihovsky and D. E. Sheehy, *Rep. Prog. Phys.* **73**, 076501 (2010).
- [36] N. Syassen, D. M. Bauer, M. Lettner, T. Volz, D. Dietze, J. J. García-Ripoll, J. I. Cirac, G. Rempe, and S. Dürr, *Science* **320**, 1329 (2008).
- [37] B. Yan, S. A. Moses, B. Gadway, J. P. Covey, K. R. A. Hazzard, A. M. Rey, D. S. Jin, and J. Ye, *Nature (London)* **501**, 521 (2013).
- [38] J. J. García-Ripoll, S. Dürr, N. Syassen, D. M. Bauer, M. Lettner, G. Rempe, and J. I. Cirac, *New J. Phys.* **11**, 013053 (2009).
- [39] L. S. Schulman, *Phys. Rev. A* **57**, 1509 (1998).
- [40] E. Altman, E. Demler, and M. D. Lukin, *Phys. Rev. A* **70**, 013603 (2004).
- [41] M. Greiner, C. A. Regal, J. T. Stewart, and D. S. Jin, *Phys. Rev. Lett.* **94**, 110401 (2005).